Extended dynamic Mott transition in the two-band Hubbard model out of equilibrium

note finali coverpage

(Article begins on next page)

23 April 2024

Extended dynamic Mott transition in the two-band Hubbard model out of equilibrium

Malte Behrmann,[1,2] Michele Fabrizio,[3] and Frank Lechermann[1]

[1]*I. Institut für Theoretische Physik, Universität Hamburg, 20355 Hamburg, Germany*
[2]*The Hamburg Centre for Ultrafast Imaging, Luruper Chaussee 149, 22761 Hamburg, Germany*
[3]*International School for Advanced Studies (SISSA), 34136 Trieste, Italy*

We reformulate the time-dependent Gutzwiller approximation by M. Schiró and M. Fabrizio [Phys. Rev. Lett. **105**, 076401 (2010)] in the framework of slave-boson mean-field theory, which is used to investigate the dynamical Mott transition of the generic two-band Hubbard model at half filling upon an interaction quench. Interorbital fluctuations lead to notable changes with respect to the single-band case. The singular dynamical transition is replaced by a broad regime of long-lived fluctuations between metallic and insulating states, accompanied by intriguing precursor behavior. A mapping to a spin model proves helpful to analyze the different regions in terms of the evolution of an Ising-like order parameter. Contrary to the static case, singlet occupations remain vital in the Mott-insulating regime with finite Hund's exchange.

Introduction.— Enormous advances in the physics of ultracold gases [1, 2] have evoked strong interest in time-dependent (TD) phenomena, which can be provoked and studied in trapped cold atom systems without all the complications that instead arise in solid-state materials. This gives the unique opportunity to investigate physical realizations of prototypical models for interacting particles, such as Bose or Fermi Hubbard models, and examine fundamental questions not only at equilibrium [3] but also in out-of-equilibrium conditions. [4–6] The simplest protocol to drive a system out of equilibrium is a sudden change of its Hamiltonian parameters, for instance an interaction quench. An intriguing issue thereof is the possible trapping within metastable configurations that have no stable equilibrium counterpart. [4, 7–10] Eventually, these metastable states decay at long times into some thermal configuration; i.e., thermalization occurs. The detailed influence of thermalization onto TD phenomena is a subject of its own. [4, 11–14] Considering the simple Fermi Hubbard model, most investigations concentrated so far on the single-orbital case. [11, 15] However, materials in nature are most often ruled by multiorbital degrees of freedom. To what extent multiorbital processes modify the encountered single-orbital Hubbard physics out of equilibrium is a highly relevant question.

In this work we report on qualitative new physics close to the dynamic Mott transition of the canonical two-band Hubbard model upon an interaction quench. The singular dynamic Mott transition in the single-band case is smeared out to a broad region with long-time fluctuations between metal and insulator. Unique precursor behavior takes place at the borders of this region.

Theoretical approach and model.— The dynamic Hubbard model is solved within TD slave-boson mean-field theory (SBMFT) that merges the rotational invariant equilibrium slave-boson method [16–18] with a nonequilibrium scheme recently proposed by Schiró and Fabrizio [15, 19, 20] via the Gutzwiller representation. [21]

In the latter scope the time evolution is described via coupled first-order differential equations for Slater determinants ψ_0 and Gutzwiller projectors ϕ; i.e.,

$$\imath|\dot{\psi}_0\rangle = \tilde{H}[\phi]\,|\psi_0\rangle \ , \tag{1}$$

$$\imath\frac{\partial\phi}{\partial t} = \mathcal{H}^{\mathrm{loc}}\,\phi + \frac{\partial\,\langle\psi_0|\tilde{H}[\phi]|\psi_0\rangle}{\partial\phi^\dagger} \ , \tag{2}$$

whereby $\tilde{H}[\phi]$ denotes the renormalized free Hamiltonian and $\mathcal{H}^{\mathrm{loc}}$ the local interacting one (note that explicit site dependance is omitted). To reexpress these equations in SBMFT a unitary transformation of the Slater determinants $|\psi_0\rangle$ into eigenstates $\nu^{\mathbf{k}}$ of $\tilde{H}[\phi]$ in momentum ($\mathbf{k}$) space is performed. Hence the former eigenstates are identified with the quasiparticle (QP) degrees of freedom. For the complete transformation, utilizing a, b for the eigenvalue labeling and A, B, C for the local basis states, one obtains

$$\imath\frac{\partial\nu_{a\alpha}^{\mathbf{k}}}{\partial t} = \sum_\beta \tilde{H}_{\alpha\beta}^{\mathbf{k}}\nu_{a\beta}^{\mathbf{k}} \ , \quad \tilde{H}_{\alpha\beta}^{\mathbf{k}} = \sum_{\alpha'\beta'} R_{\alpha\alpha'}^\dagger \varepsilon_{\alpha'\beta'}^{\mathbf{k}} R_{\beta'\beta} \ , \tag{3}$$

$$\imath\frac{\partial\phi_{AB}}{\partial t} = \sum_C \mathcal{H}_{AC}^{\mathrm{loc}}\phi_{CB} + \sum_{\mathbf{k}b}^{\mathrm{occ}}\sum_{\alpha\beta} \nu_{b\alpha}^{*\mathbf{k}}\frac{\partial\tilde{H}_{\alpha\beta}^{\mathbf{k}}}{\partial\phi_{AB}^\dagger}\nu_{b\beta}^{\mathbf{k}} \ . \tag{4}$$

with α, β denoting the respective orbital-spin combination. The matrices $R_{\alpha\alpha'}=R_{\alpha\alpha'}[\phi]$ renormalize the free dispersion $\varepsilon_{\alpha\beta}^{\mathbf{k}}$ and form the QP-weight matrix $\mathbf{Z}=\mathbf{R}\mathbf{R}^\dagger$. [17] Equations (3) and (4) show the coupled time evolution of QP states $\nu^{\mathbf{k}}$ and local slave-boson amplitudes ϕ_{AB}. Within mean-field versions of Gutzwiller and slave-boson techniques, those quantities are subject to certain constraints, reading (for each point in time t)

$$\mathrm{Tr}\left(\phi^\dagger\phi\right) = 1 \ , \quad \mathrm{Tr}\left(\phi^\dagger\phi\,c_\alpha^\dagger c_\beta\right) = \sum_{\mathbf{k}b}^{occ} \nu_{b\alpha}^{*\mathbf{k}}\nu_{b\beta}^{\mathbf{k}} \ . \tag{5}$$

A numerical solution of Eqs. (3) and (4) is achieved by using an adaptive Runge-Kutta scheme of order 5/6. [22]
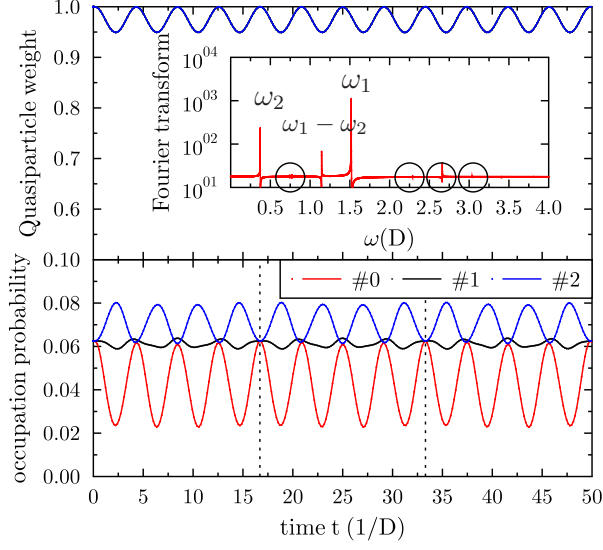
FIG. 1. (Color online) QP weight $Z(t)$ and occupation probability $\#p$ of local sectors with particles $p=0,1,2$ for the interaction quench to $U_f=0.2$. Dotted lines denote period of local states oscillations. The inset shows the Fourier transform (absolute value of Fourier coefficients in logarithmic units) of $Z(t)$. See the text for use of the circles.

We study the canonical two-band Hubbard Hamiltonian $\mathcal{H} = H + \sum_i \mathcal{H}_i^{\text{loc}}$ with a nearest-neighbor hopping τ that defines the kinetic part H. In detail it reads

$$\mathcal{H} = -\tau \sum_{\langle i,j \rangle m\sigma} \left(c_{im\sigma}^\dagger c_{jm\sigma} + \text{h.c.} \right) + U \sum_{im} n_{im\uparrow} n_{im\downarrow} +$$

$$+ \frac{1}{2} \sum_{i, m \neq m', \sigma} \left\{ U' n_{im\sigma} n_{im'\bar{\sigma}} + U'' n_{im\sigma} n_{im'\sigma} + \right. \qquad (6)$$

$$\left. + J \left(c_{im\sigma}^\dagger c_{im'\bar{\sigma}}^\dagger c_{im\bar{\sigma}} c_{im'\sigma} + c_{im\sigma}^\dagger c_{im\bar{\sigma}}^\dagger c_{im'\bar{\sigma}} c_{im'\sigma} \right) \right\},$$

where i, j are site indices, m, m' run over orbitals 1, 2, and $\sigma=\uparrow,\downarrow$ marks the spin projection, i.e., $\alpha, \beta = m\sigma, m'\sigma$ in connection with (3) and (4). A three-dimensional simple-cubic dispersion is used and thus the parametrization $U'=U-2J$, $U''=U-3J$ proves adequate. [23, 24] The value of the hopping τ is such that the half-bandwidth D is the energy unit. To investigate an interaction quench the initial U_i is set to zero and the local interaction varies in time as $U(t)=U_f \Theta(t)$ and $J(t)=qU_f \Theta(t)$, i.e., jumps from zero to U_f and qU_f at $t=0$. In the following we focus on the paramagnetic half-filled scenario and aim at general dynamic multiorbital Mott-transition mechanisms; thus antiferromagnetic fluctuations on the specifically chosen lattice type are neglected.

Results.— First the limiting case $J=0$ $(q=0)$, i.e., $U=U'=U''$, is examined. The quench leads to nonvanishing oscillations in the physical observables due to the lack of quantum fluctuations in the present formalism. [15] In Fig. 1 the TD QP weight $Z_{m\sigma}(t)=\delta_{12}\delta_{\uparrow\downarrow}Z(t)$ and occupation probability $\#p$ of local particle sectors is dis-

played for small U_f. While $Z(t)$ and the occupation in the $p=0,1$ sectors oscillate in phase, the two-particle sector commutes with a π phase shift thereto. As expected, minima in $Z(t)$ amount to maxima in $\#2$ and vice versa. The Fourier transform (inset in Fig. 1) reveals the occurrence of two main frequencies ω_1, ω_2 as well as sidebands. This is in contrast to the single-band and the quasi-decoupled ($U'=U''=0$) two-band case, where only a single frequency on the order of ω_1 shows up. While the latter frequency in the fully interacting case is sensitive to changes in the hopping τ, ω_2 remains rather unaffected. Hence ω_2 originates from interorbital processes and is absent for the quasi-decoupled-band case. The encircled frequencies are integer multiples of ω_1, ω_2 or sidebands and appear due to Fourier transformation on a finite-time interval (note logarithmic units). The time interval was set to $7500 \, D^{-1}$ to provide suitable high-frequency resolution $<(1000D)^{-1}$.

The overall relevant-frequency behavior from the Fourier transform of $Z(t)$ with increasing U_f is depicted in Fig. 2 with comparison to the $U'=U''=0$ case. For the latter, the bands are independent and we recover the results of the single-band study. [15] A dynamic Mott transition occurs at $U_c^{(1)}=1.325$ eV indicated by a logarithmic divergence in the single frequency ω_{1S}, smeared out due to the numerical integration. With interorbital terms, multiple relevant frequencies appear with growing
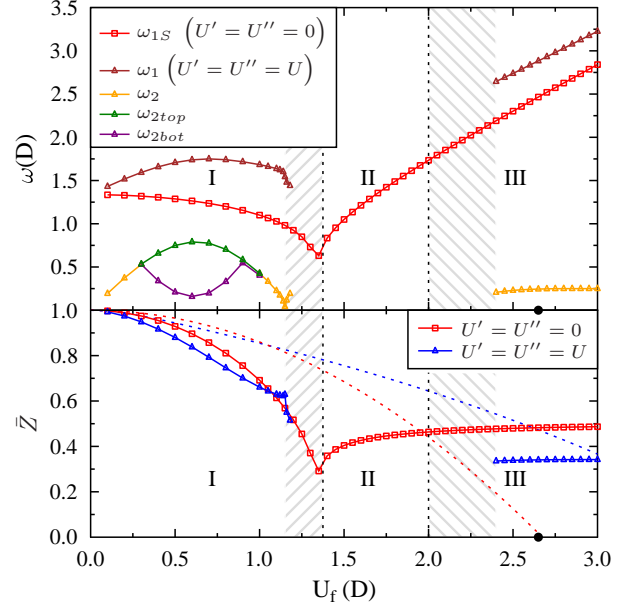

FIG. 2. (Color online) Top: Main-frequency evolution with U_f for $U'=U''=0$ and $U'=U''=U$ from Fourier transforming $Z(t)$. The dotted lines separate three different regions (see text and Fig. 4). Bottom: Time-averaged Z as a function of U_f. Dashed lines mark the equilibrium behavior with the black dot denoting the associated Mott-critical point. Gray hashed area indicates precursor behavior.
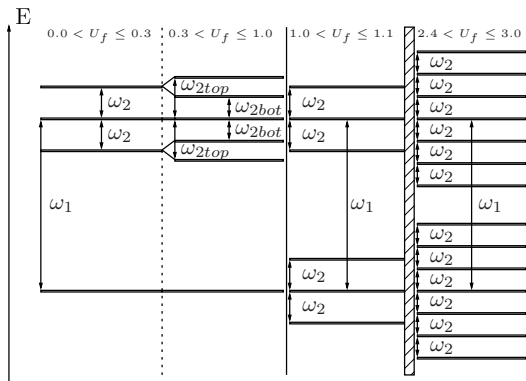
FIG. 3. Level diagram for the active frequencies in the case $U'=U''=U$ within the different regimes dictated by U_f.
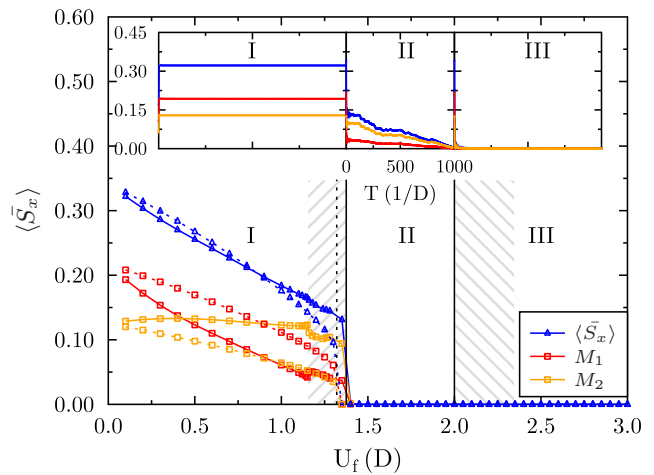

FIG. 4. (Color online) Order parameter $\langle \bar{S}_x \rangle$ for $U'=U''=0$ (dashed) and $U'=U''=U$ (full). Inset shows $\langle \bar{S}_x \rangle (T)$ in the three different regions. The quasidecoupled two-band case stabilizes only in regions I and III (divided by the vertical dashed line). Region II appears with interorbital terms. The precursor regime is visualized by the gray hashed area.

U_f. In fact, ω_2 consists of two coupled interorbital contributions, namely ω_{2top} and ω_{2bot}. Both contributions tend to zero close to the dynamic Mott criticality, which we believe to occur near $U_c^{(1)}$ (see below). Three observations from Fig. 2 are vital. The first is the splitting of ω_2 for $0.3 < U_f < 1.0$ which can be visualized within a level scheme (see Fig. 3). That scheme shows the onset of splitting between levels connected by ω_1 when approaching the Mott critical regime. The second is that a broad region of mostly noisy Fourier spectra appears for $1.15 < U_f < 2.375$ without a clear structuring. Albeit already insulating, a definite level structure then reemerges for $U_f > 2.375$.

Whereas ω_2 saturates for large interaction quenches, ω_1 linearly rises with the same slope as in the quasidecoupled-bands case. Figure 2 also shows the quantity $\bar{Z} = \bar{Z}(T) \equiv \frac{1}{T} \int_0^T dt\, Z$, based on time-averaging over a long-time interval T (not to be confused with a basic period of oscillation), in comparison with the equilibrium QP weight. If not specified T was set to $7500\ D^{-1}$. A well-defined $\bar{Z}$ is only accessible outside the broad U_f range with noisy Fourier spectrum. Interestingly, just before entering the latter regime a small range appears where $\bar{Z}$ of the $U'=U''=0$ model is *smaller* than in the one with including interorbital terms. Thus interorbital interactions allow one to *reduce* the standard correlation measure in certain out-of-equilibrium cases.

Better understanding of the dynamical transition at $J=0$ can be gained by an Ising-spin representation of the model that is fully equivalent to slave-bosons and reads [19]

$$\mathcal{H}_S = -\frac{J}{S^2}\frac{2}{r}\sum_{\langle i,j \rangle} S_{ix}S_{jx} + \frac{U}{2}\sum_i (S_{iz})^2 \quad , \quad (7)$$

with spin $S=2$ and where $r=6$ is the lattice coordination number while $-J=-2/3$ is the energy per site of the non interacting ground state. Within mean field, i.e., assuming a variational wave function $\prod_i |\Phi(S_{iz})\rangle$, the spin

model above becomes identical to the slave-boson mean-field theory at half filling if $|\Phi(S_{iz})\rangle = \sum_{p=0}^4 \phi_p\, |S_{iz} = p-2\rangle$, where ϕ_p is the original slave boson at site in particle sector p. Because of half filling, $\phi_p = \phi_{4-p}$, so that $\langle S_{iz} \rangle = 0$. Metallic coherence is signaled in the spin model by a finite Ising order parameter $\langle S_{ix} \rangle = \Re\left[\sqrt{6}\left(\phi_3^* \phi_2 + \phi_2^* \phi_1\right) + 2\left(\phi_4^* \phi_3 + \phi_1^* \phi_0\right)\right] \equiv M_1 + M_2$, while the incoherent Mott insulator has $\langle S_{ix} \rangle = \langle S_{iz}^2 \rangle = 0$. The initial noninteracting state is characterized by $\langle S_{ix} \rangle = 2$ and $\langle S_{iz}^2 \rangle = 1$, i.e. energy per site $E = -2/3 + U/2$, conserved during the unitary evolution. If, like in the single-band case, [15] we assume the dynamical Mott transition to occur when the energy equals that of the Mott insulator, i.e., $E=0$, then we would expect $U_c^{(2)} = 4/3$, which is also equal to the single-band value for the dynamical Mott transition. In fact, this argument predicts one and the same value $U_c = 4/3$ for any N-band simple, i.e., $J=0$, Hubbard model at half filling, indeed close to the numerical value.

Figure 4 exhibits the time-averaged quantity $\langle \bar{S}_x \rangle$ with increasing U_f, indeed classifying three different regions. Hence $\langle \bar{S}_x \rangle$ does serve here as an order parameter, where regime I is metallic with a finite $\langle \bar{S}_x \rangle$. However there is a crossover of the contributions $\bar{M}_1$, $\bar{M}_2$ for $U'=U''=U$, showing that correlations between local states of the one- (three-) and two-particle sectors are less affected by increasing U_f than those between zero- (four-) and one- (three-) particle sectors. For $U'=U''=0$ the order parameter jumps to zero at $U_c^{(1)}$, signaling the dynamic metal-insulator transition into a regime III. With finite interorbital interactions the behavior is surprisingly more in-
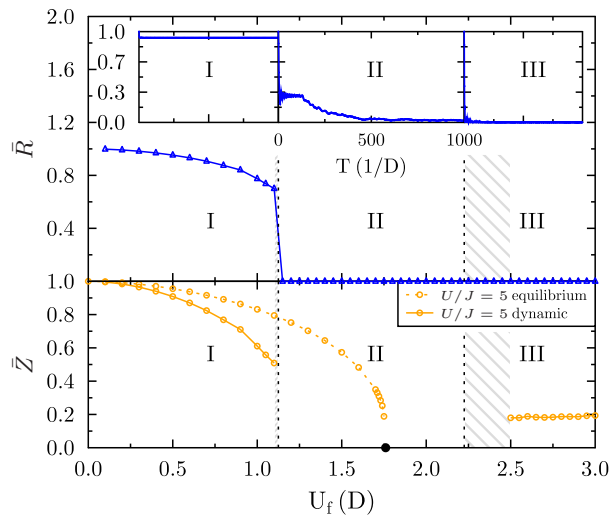
FIG. 5. (Color online) Time-averaged diagonal renormalization R and QP weight Z for $U/J = 5$. Black dot marks the Mott-critical point of the associated equilibrium model. Insets show $\bar{R}(T)$ in the three different regions.
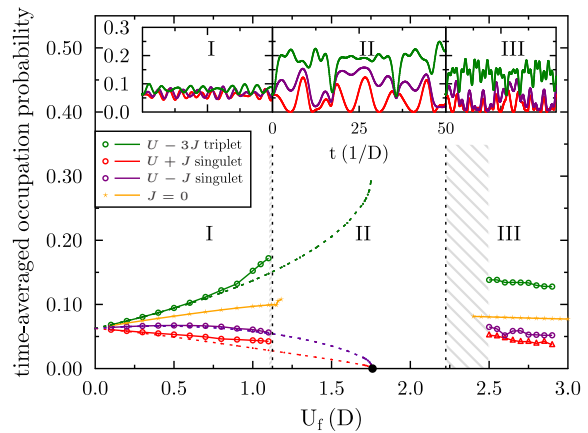

FIG. 6. (Color online) Time-averaged multiplet occupation probabilities for $U/J = 5$ with the equilibrium probabilities (dashed lines) for comparison. The Mott-critical point of the associated equilibrium model is described by a black dot. Insets reveal explicit time evolution of multiplet occupation probabilities in different regions.

triguing. At $U_f = 1.15$ a precursor regime starts with increased fluctuations of growing frequency. The integrated components M_1, M_2 are specifically sensitive thereto. This may be connected to the breakdown of ω_2 shown in Fig. 2, leading to a noncontinuous evolution of correlations between the local particle sectors. In the region $1.375 \leq U_f \leq 2.0$ the order parameter then indeed vanishes, but only after an extremely long time. This extended Mott-insulating transition (EDMT) is characterized by a chaotic-like time evolution of the QP weight and the multiplet-occupation probabilities. This is in accordance with the noisy Fourier spectra. Note that the EDMT is a unique feature of the general two-band model with interorbital interactions. The static Mott-critical interaction strongly differs if the orbitals are explicitly coupled ($U_c \sim 2.65$) or not ($U_c \sim 4.0$). In contrast the boundary of the dynamic metallic region I is quite independent of the coupling type, but a qualitative difference is introduced via the appearance of an intermediate region for interaction-coupled orbitals.

The EDMT is not an artifact of the ($J=0$) case but a general feature of the general dynamic two-band Hubbard model. Since $\langle \bar{S}_x \rangle$ is proportional to the R matrix [see Eq. (4)], the quantity $\bar{R}$ serves as a suitable order parameter in the original model and is depicted for $U/J = 1/q = 5$ [including all interaction terms in Eq. (6)] in Fig. 5. The precursor regimes as well as the occurrence of the EDMT persists. In fact with finite J this intermediate region is even broadened ($1.125 \leq U_f \leq 2.225$) in the $\bar{R}$-U_f diagram compared to the $J=0$ case ($1.375 \leq U_f \leq 2.0$). In addition, Fig. 6 shows the evolution of the time-averaged multiplet-occupation probabilities for finite J. For small U_f they are close to the values in the equilib-

rium model, but lack the strong polarization in the insulating region. While in the static case only the triplet channels survive the Mott transition, the dynamic Mott region III displays also finite singlet fillings.

Summary.— We have investigated an interaction quench in the canonical two-band Hubbard model with the TD-SBMFT scheme allowing for complete rotational invariance. The limited case with sole intraorbital interaction terms leads to a quasi decoupled two-band model with dynamic characteristics reminiscent of prior single-band studies. [15] On the other hand, when introducing the relevant interorbital interactions, novel physics appears out of equilibrium. An intermediate region with long-time chaotic-like fluctuations in the physical amplitudes and high-frequency metal-to-insulator fluctuations emerges and replaces the singular Mott-transition point. This replacement goes along with precursor regimes exhibiting high-frequency fluctuations in time. Finally the appearance of chaotic-like behavior may be connected to the non integrable classical coupled-pendulum problem, which indeed displays chaotic orbits. Extensions beyond mean field are needed to reveal whether such analogies hold in the complete quantum-fluctuating scenario.

[1] I. Bloch, J. Dalibard, and W. Zwerger, Reviews of Modern Physics **80**, 885 (2008).

[2] S. Giorgini, L. P. Pitaevskii, and S. Stringari, Reviews of Modern Physics **80**, 1215 (2008).

[3] R. Jördens, N. Strohmaier, K. Günter, H. Moritz, and T. Esslinger, Nature **455**, 204 (2008).

[4] A. Polkovnikov, K. Sengupta, A. Silva, and M. Vengalattore, Reviews of Modern Physics **83**, 863 (2011).

[5] M. J. Mark, E. Haller, K. Lauber, J. G. Danzl, A. Janisch, H. P. Büchler, A. J. Daley, and H.-C. Nägerl, Physical Review Letters **108**, 215302 (2012).

[6] S. Trotzky, Y.-A. Chen, A. Flesch, I. P. McCulloch, U. Schollwöck, J. Eisert, and I. Bloch, Nature Physics (2012), 10.1038/nphys2232.

[7] M. Eckstein and M. Kollar, Physical Review Letters **100**, 120404 (2008).

[8] P. Werner and M. Eckstein, Physical Review B **86**, 045119 (2012).

[9] M. Kollar, F. A. Wolf, and M. Eckstein, Physical Review B **84**, 054304 (2011).

[10] G. Carleo, F. Becca, M. Schiró, and M. Fabrizio, Scientific Reports **2** (2012), 10.1038/srep00243.

[11] M. Eckstein, M. Kollar, and P. Werner, Physical Review Letters **103**, 056403 (2009).

[12] B. Sciolla and G. Biroli, Link arXiv e-print 1211.2572 (2012).

[13] C. Ates, J. P. Garrahan, and I. Lesanovsky, Physical Review Letters **108**, 110603 (2012).

[14] E. Canovi, D. Rossini, R. Fazio, G. E. Santoro, and A. Silva, Physical Review B **83**, 094431 (2011).

[15] M. Schiró and M. Fabrizio, Physical Review Letters **105**, 076401 (2010).

[16] T. Li, P. Wölfle, and P. J. Hirschfeld, Physical Review B **40**, 6817 (1989).

[17] F. Lechermann, A. Georges, G. Kotliar, and O. Parcollet, Physical Review B **76**, 155102 (2007).

[18] A. Isidori and M. Capone, Physical Review B **80**, 115120 (2009).

[19] M. Fabrizio, Link arXiv e-print 1204.2175 (2012).

[20] M. Schiró and M. Fabrizio, Physical Review B **83**, 165105 (2011).

[21] A variant of the TD Gutzwiller technique was introduced [25] to compute response functions and has recently been extended [26].

[22] J. Verner, Numerical Algorithms **53**, 383 (2010).

[23] C. Castellani, C. R. Natoli, and J. Ranninger, Physical Review B **18**, 4945 (1978).

[24] R. Frésard and G. Kotliar, Physical Review B **56**, 12909 (1997).

[25] E. v. Oelsen, G. Seibold, and J. Bünemann, Physical Review Letters **107**, 076402 (2011).

[26] J. Bünemann, M. Capone, J. Lorenzana, and G. Seibold, New Journal of Physics **15**, 053050 (2013).